Measuring the acoustoelectric interaction constant using ultrasound current source density imaging

2012 Phys. Med. Biol. 57 5929

(http://iopscience.iop.org/0031-9155/57/19/5929)

IOP PUBLISHING PHYSICS IN MEDICINE AND BIOLOGY

Phys. Med. Biol. **57** (2012) 5929–5941 doi:10.1088/0031-9155/57/19/5929

Measuring the acoustoelectric interaction constant using ultrasound current source density imaging

Qian Li[1], **Ragnar Olafsson**[2], **Pier Ingram**[1], **Zhaohui Wang**[3] **and Russell Witte**[1]

[1] Department of Medical Imaging, University of Arizona, Tucson, AZ 85724, USA
[2] Department of Electrical and Computer Engineering, University of Iceland, Iceland
[3] Department of Medicine, University of Pittsburgh, Pittsburgh, PA 15260, USA

E-mail: qianl@email.arizona.edu

Received 2 May 2012, in final form 13 July 2012
Published 7 September 2012
Online at stacks.iop.org/PMB/57/5929

Abstract

Ultrasound current source density imaging (UCSDI) exploits the acoustoelectric (AE) effect, an interaction between ultrasound pressure and electrical resistivity, to map electrical conduction in the heart. The conversion efficiency for UCSDI is determined by the AE interaction constant K, a fundamental property of all materials; K directly affects the magnitude of the detected voltage signal in UCSDI. This paper describes a technique for measuring K in biological tissue, and reports its value for the first time in cadaver hearts. A custom chamber was designed and fabricated to control the geometry for estimating K, which was measured in different ionic salt solutions and seven cadaver rabbit hearts. We found K to be strongly dependent on concentration for the divalent salt $CuSO_4$, but not for the monovalent salt NaCl, consistent with their different chemical properties. In the rabbit heart, K was determined to be $0.041 \pm 0.012\%/\text{MPa}$, similar to the measurement of K in physiological saline ($0.034 \pm 0.003\%/\text{MPa}$). This study provides a baseline estimate of K for modeling and experimental studies that involve UCSDI to map cardiac conduction and reentry currents associated with arrhythmias.

(Some figures may appear in colour only in the online journal)

1. Introduction

Cardiac catheter ablation has evolved to be a standard clinical treatment for arrhythmia. The procedure requires mapping the heart's electrical system prior to ablation. Traditional electrophysiology (EP) mapping is now standard, although the technique has certain shortcomings. For instance, fluoroscopy is often used to track the position of the catheter, exposing both the patient and operator to ionizing radiation. Advanced mapping technologies, like electro-anatomical mapping (EAM), have been introduced in the last decade to facilitate

the mapping of the cardiac activation wave and identifying reentry currents (Markides and Davies 2005, Packer 2005). Despite the high technological success and widespread acceptance of the procedure for clinical practice, there are factors limiting its functionality. For example, commercial mapping systems, such as the CARTO^{TM} EAM system, are prone to registration errors and not able to monitor the cardiac activation wave in real time, require multiple averages of the ECG and, consequently, not able to detect non-sustained arrhythmias (e.g., ventricular tachycardia) (Duru 2002, Markides and Davies 2005).

To overcome limitations of traditional methods, we have formerly proposed ultrasound current source density imaging (UCSDI) as a new technology for mapping bio-potentials in the human heart to detect arrhythmias (Olafsson *et al* 2009), or, in the brain, mapping epileptic foci (Witte *et al* 2007, Olafsson *et al* 2008). UCSDI can achieve 4D imaging (volume + time) with superior spatial resolution and minimal invasiveness using as few as one recording electrode and reference (Wang *et al* 2010).

UCSDI is based on Ohm's law and the acoustoelectric (AE) effect, which can be described as

$$\frac{\Delta\rho}{\rho_0} = -K\Delta P, \tag{1}$$

where $\Delta\rho$ is the resistivity change, ρ_0 the direct current resistivity, ΔP the ultrasonic pressure and K the interaction constant. In other words, the AE effect is a change in resistivity induced by a change in local pressure. The conversion efficiency is determined by K, which is a property of all materials. The AE effect was first reported in the 1940s (Fox *et al* 1946) and later used for electrical tomography with potential cancer applications (Zhang and Wang 2004, Gendron *et al* 2009).

For UCSDI, the AE effect modulates a material's resistivity exclusively at the focal spot of an ultrasound beam. The AE signal recorded on a bioelectrode is simultaneously co-registered with the pulse echo (PE) signal detected by the ultrasound transducer. The degree of the modulation is affected by the interaction constant K. From equation (1), it is clear that the amplitude of the AE signal is proportional to K. While K has been assessed in electrolytes (e.g., a typical value in 0.9% NaCl solution was reported to be on the order of 0.01–0.1%/MPa) (Jossinet *et al* 1998, 1999, Lavandier *et al* 2000a, 2000b), the value has not been calculated in many other types of material, including biological tissue.

Owing to its importance to UCSDI for cardiac imaging, we developed a system and apparatus to measure K in electrolytes and rabbit heart tissue. The magnitudes of the AE signal and interaction constant were measured in strips of rabbit heart tissue, as well as in different concentrations of NaCl and $CuSO_4$ solution. These two salts were chosen because of their different ionic composition and chemical properties. In aqueous salt solution, the AE effect occurs through the variation of the parameters controlling the ionic resistivity against pressure and temperature. NaCl is a monovalent salt, in which the AE effect was found to be almost independent of concentration; $CuSO_4$ is a divalent salt whose AE behavior was hypothesized to rely on concentration, yet never proven experimentally (Koerber 1909). An accurate estimate of K would provide a baseline for detecting the AE signal in cardiac tissue, thereby enabling us to build better models and optimize UCSDI instrumentation toward clinical use.

2. Theory

As illustrated in figure 1, when current is flowing through the material, the change in resistivity can be measured, according to Ohm's law, in the form of a voltage variation. On a 2D plane,

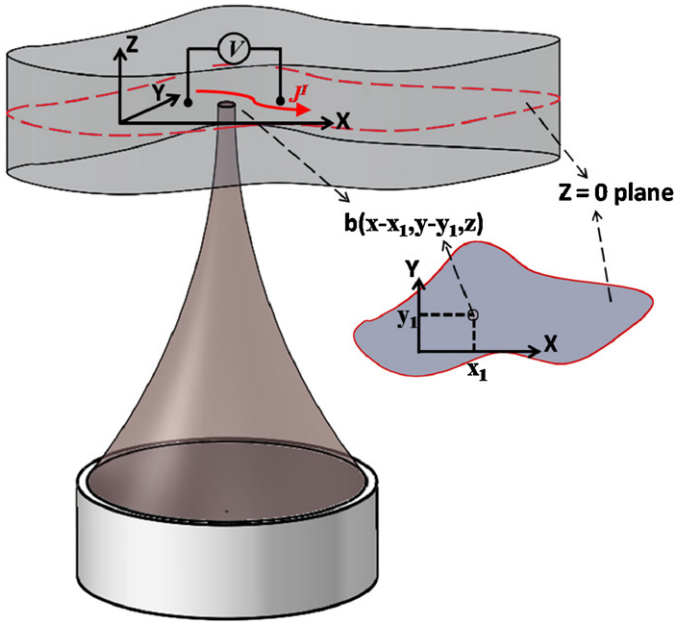

Figure 1. Illustration of the key physical components affecting UCSDI. Assume the ultrasound focus, recording electrode leads and the biological current are all on the same plane $Z = 0$ inside a volume conductor. Biological current density is J^I. One pair of leads measures the injected voltage (low frequency) and the induced AE voltage (high frequency). V denotes a voltage detector. The beam pattern is $b(x–x_1, y–y_1, z)$ with the coordinate of the ultrasound focus (center of the ultrasound beam profile in $Z = 0$ plane) being $(x_1, y_1, 0)$.

this voltage change can be expressed as

$$V^{\mathrm{AE}}(x_{1,}y_{1,}t) = -K\rho_0 \iiint (\tilde{J}^L \bullet J^I)\Delta P b(x - x_{1,}y - y_{1,}z)a\left(t - \frac{z}{c}\,\mathrm{d}x\,\mathrm{d}y\,\mathrm{d}z\right), \tag{2}$$

where V^{AE} is the ultrasound modulated voltage change, that is, the AE signal measured by an electrode relative to a reference, $\tilde{J}^L$ is the lead vector field of the electrode and J^I is the propagating biological current source; $b\,(x - x_1, \quad y - y_1, \quad z)$ is the beam pattern of the ultrasound transducer and $a(t - z/c)$ is the pulse waveform. In this representation, ρ_0 is assumed to be constant over the extent of the ultrasound wavepacket. A full derivation of (2) and detailed discussion can be found in another publication (Olafsson *et al* 2008). Thus, the AE signal is localized at the focal region of the ultrasound beam. When the beam is scanned mechanically or electronically, a collection of AE signals is detected to form images proportional to the local current densities. PE ultrasound can be acquired simultaneously for structural information and co-registering with UCSDI.

The interaction constant K is a fundamental material property affecting the magnitude of the AE signal. Figure 2 portrays the steps for calculating K based on the detected AE signal using UCSDI. Assume that the material has a rectangular shape and is illuminated by an ultrasound beam traveling in the Z direction. The resistivity of the material within the focal region is modulated by $\Delta\rho$ according to (1), and thus is $\Delta\rho+\rho_0$, with ρ_0 being the resistivity

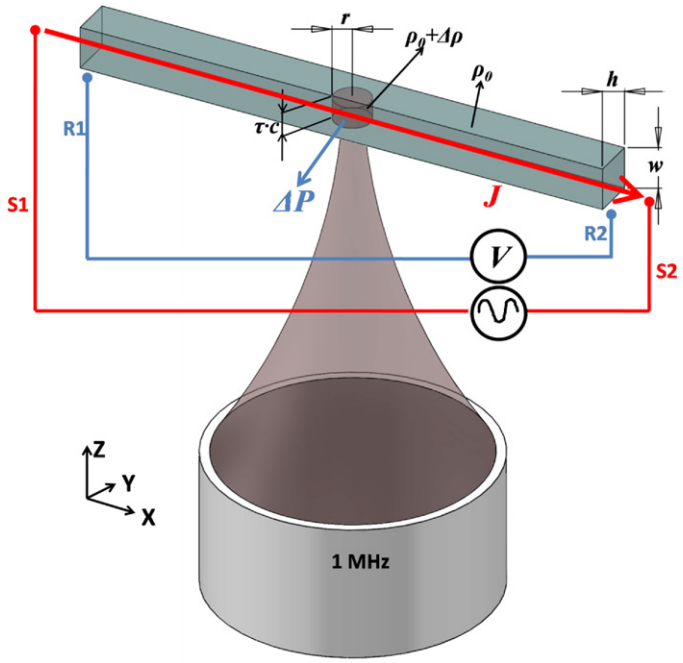

Figure 2. Generation and detection of AE signal for calculating K. Transducer sends pulsed ultrasound to a rectangular-shaped material at a distance of one focal length. The width and height of the material are w and h respectively. r is the beam radius measured at the focus using a calibrated hydrophone. The ultrasound pulse was taken to have a rectangular shape in the Z direction, where the pressure amplitude is ΔP at the focal zone with a duration τ and zero everywhere else. c is the velocity of sound in water; so $\tau \cdot c$ determines the length of the focal zone in the Z direction. ρ_0 is the resistivity of the material and $\Delta\rho$ the ultrasound induced resistivity change of the material. A function generator with certain output voltage injects current with density J through the material with stimulating electrodes S1 and S2. R1 and R2 are the recording electrodes, which detect the AE signal.

in the volume not affected by ultrasound. $\Delta\rho$ can be calculated based on the geometry defined in figure 2 using a simple circuit model. Inserting the calculated $\Delta\rho$ into (1) yields

$$K = \underbrace{-\left(\frac{h}{2r}\right)^2 \frac{w^2}{\tau c}\frac{\pi}{2}}_{\text{I}} \underbrace{\frac{1}{\rho_0}\frac{\Delta R}{\Delta P}}_{\text{II}}, \tag{3}$$

where part I comes from the geometry defined in figure 2 and part II is calculated based on the experimental measurement. In part II, ΔP is the ultrasonic pressure at focus, ρ_0 the resistivity of the material and ΔR the change in resistance due to the modulation by ultrasound.

The original derivation of (3) was described by Jossinet *et al* (2000), and, in a preliminary study, we used a similar approach to calculate K in ionic solutions and cardiac tissue (Li *et al* 2010).

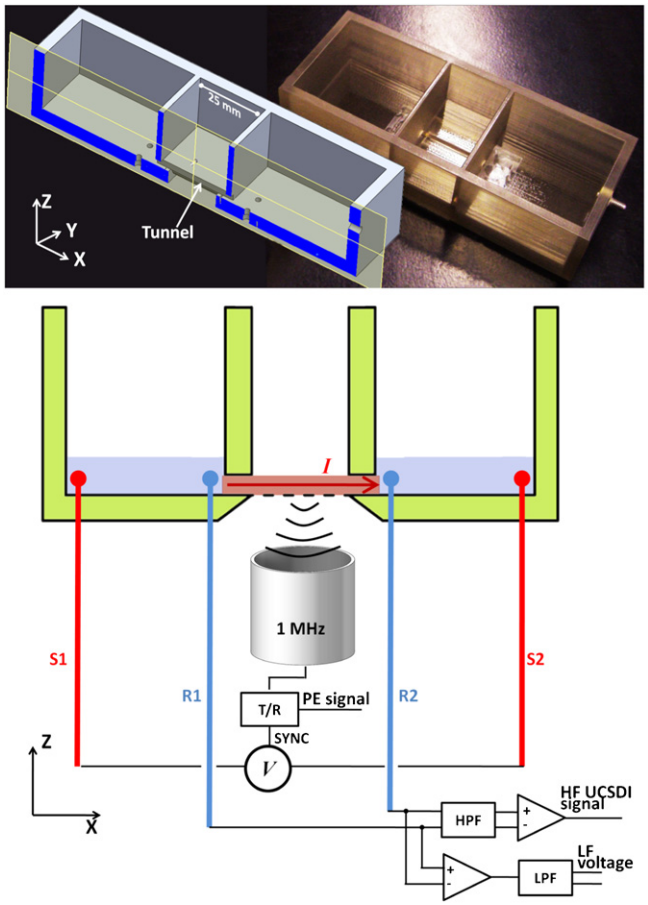

Figure 3. Top: the *X*–*Z* cross-section view of the initial design of the chamber (left) and actual photograph (right). The chamber has three compartments that are electrically coupled: two side compartments for electrolyte and a middle compartment containing a tunnel for placement of the samples. Bottom: instrumentation for measuring *K*. T/R: ultrasound pulser/receiver, which was pulsed in synchrony with the function generator. HPF: high pass filter. LPF: low pass filter. LF: low frequency. HF: high frequency.

3. Methods and materials

3.1. Chamber for measuring K in electrolytes and biological tissue

A custom chamber was fabricated to control the geometry for measuring the interaction constant *K* (figure 3, top). The initial design was generated using SolidWorks® based on the geometry defined in figure 2 and then fabricated using a 3D rapid prototyping machine (Objet Connex350). The chamber featured three compartments. Two side compartments contained electrolyte solution (NaCl or $CuSO_4$) for electrical coupling of the sample to the current-injecting electrodes. The middle compartment included a rectangular tunnel for holding the sample and confining current flow. The inner dimensions of the tunnel (2.5 mm $\times$ 2.5 mm $\times$ 25mm) were carefully chosen to fit the geometrical model described in figure 2 and equation (3). The bottom of the tunnel was an acoustic window made of Tegaderm™.

3.2. Imaging system and apparatus for measuring AE interaction constant

As depicted at the bottom of figure 3, one pair of platinum electrodes (S1 and S2) connected to a signal generator (Agilent, 33220A) was used to directly pass alternating current at 200 Hz through the sample in the tunnel. Voltage was measured across a 1 Ω resistor placed in series with one of the current-injecting electrodes to determine the current amplitude. Another pair of Ag/AgCl electrodes (R1 and R2) recorded the signal, which was bifurcated and fed into two differential amplifiers. One amplifier (Lecroy 1855, 20 MHz bandwidth) was connected to an analogue high pass filter (200 kHz cut-off-frequency) to record the high frequency AE signal, which was further amplified and captured on a fast 12-bit acquisition board (Signatec, PDA12, 60 MHz bandwidth) with a total gain of 54 dB. A second differential amplifier (Lecroy 1855, 100 kHz bandwidth) captured the low frequency voltage signal, which was recorded on a separate data acquisition system (National Instruments BNC-2110) and was used to calculate the resistivity ρ_0 in (2). A 1 MHz single element focused transducer (Panametrics, $f = 68$ mm, $D = 41$ mm) was pulsed in synchrony with the peak and trough of the 200 Hz current injection. The PE signal received by the transducer was also simultaneously recorded using the PDA12. To obtain PE and AE signals at each position in the tunnel, the transducer was raster scanned (Velmex PK245–01AA) to produce 3D UCSDI and PE images. A 3D UCSDI image is essentially a collection of AE signals at each position to produce a 3D current source density image of the tunnel. Pressure at the focus in the tunnel was measured with a calibrated hydrophone (Onda, HGL-0200).

3.3. Signal processing and data analysis

The AE signals detected at the peak and trough of the current injection were averaged 100 times and then subtracted from each other to reduce common-mode noise. The subtracted signals were then bandpass filtered according to the frequency response of the transducer. The simultaneously recorded PE signals based on two-way travel of the acoustic wave detected by the transducer were processed in a similar fashion. The AE and PE signals were then demodulated to produce the envelope for analysis and display.

The baseline resistivity ρ_0 was calculated from the low frequency voltage recording. The change in resistance ΔR of the samples due to the pressure pulses was calculated from the slope of recorded AE voltage at various current levels. Linear fitting of the resistance and the pressure gave $\Delta R/\Delta P$. Part II of (3), $(\Delta R/\Delta P)/\rho_0$, was then calculated and combined with the measured part I to determine K.

3.4. Animal preparation and materials

K was measured in rabbit heart tissue and electrolytes for comparison. Seven fresh rabbit hearts were obtained according to protocols approved by the Institutional Animal Care and Use Committee (IACUC) at the University of Arizona. Adult New Zealand White rabbits were sacrificed by intracardiac administration of Beuthanasia® (1 cc/10 lb) after anesthetization by intramuscular injection of a mixture of ketamine and xylazine. Immediately after the rabbit was euthanized, the heart was excised and immersed in 0.9% phosphate buffered saline. A segment of tissue was removed with a scalpel along the long axis of the left ventricle. The excised strip of tissue had dimensions very close to the size of the tunnel (2.5 mm × 2.5 mm × 25 mm), such that the tissue conformed to the shape of the tunnel. 0.9% phosphate buffered saline was added to the side compartments, submerging the electrodes.

For the first five rabbit hearts, experiments for determining K were performed at room temperature (24 °C). Another heart was used to track the variability of K, also at 24 °C, during

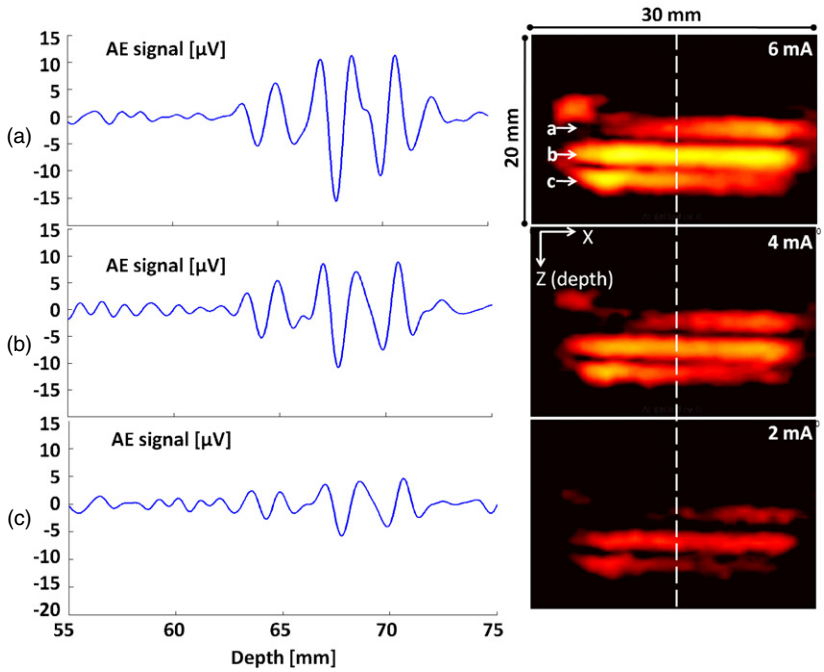

Figure 4. AE signals and UCSDI images from 0.9% NaCl at different current levels. Left: traces of AE signal associated with the position marked by white dashed line on the right. Right: UCSDI images of the tunnel filled with 0.9% NaCl at current levels of 6, 4 and 2 mA. Arrow 'a' points to the solution–membrane interface, 'b' the solution–air interface and 'c' an artifact caused by the reflection of the acoustic wave.

several hours of recording immediately after tissue extraction. This ensured that the tissue was fresh and its physical properties were not changing appreciably during the measurement of K. In addition, because initial experiments were performed at 24 °C, we also wanted to examine the effect of temperature on the measurement of K in cardiac tissue between room and body temperature. Tissue temperature was controlled by heating and cooling the surrounding saline bath. Temperature was monitored using a calibrated k-type thermocouple in contact with the tissue. The value of K was measured between 23 and 41 °C.

For comparing K in different electrolytes, the side compartments and tunnel were filled with either NaCl (monovalent) or $CuSO_4$ (divalent) solutions. To determine the concentration dependence of K for these different salt solutions, K was measured for five different concentrations (0.3%, 0.6%, 0.9%, 1.2% and 1.5%) of each salt at 24 °C.

4. Results

4.1. K in electrolytes

Figure 4 displays the AE signals (left) recorded from 0.9% saline for three different current levels and the UCSDI images (right) formed from the AE signals along the scan distance. The AE signals are radiofrequency traces corresponding to the position at the white dashed line in the UCSDI images. The effect of different current amplitudes on the AE signal is manifested. As the current amplitude decreased, the AE signal also decreased proportionally.

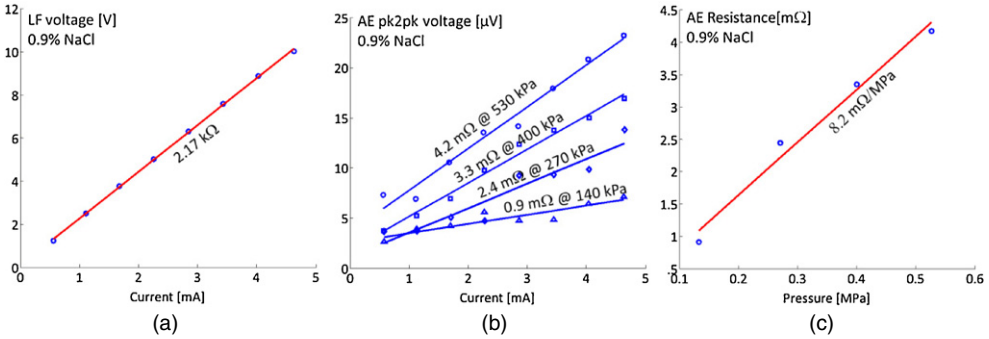

Figure 5. Calculation of K in 0.9% NaCl. (a) LF voltage at different current injections is plotted to obtain the slope (2.17 kΩ), which is the LF resistance. (b) At pressure levels of 140, 270, 400 and 530 kPa, AE peak-to-peak amplitude at different current injections is plotted to obtain the slopes, which are 0.9, 2.4, 3.3 and 4.2 mΩ, respectively. (c) The four AE resistances at each pressure from (b) are linear fitted to obtain $\Delta R/\Delta P$.

We use 0.9% NaCl here as an example to demonstrate the process for calculating K. In figure 5(a), the slope of low frequency voltage at various current levels provided the low frequency resistance R_0, which was used to calculate ρ_0 given the geometry defined in figure 2. Best fit lines of the AE voltages recorded at multiple current amplitudes at a particular pressure were used to calculate the AE resistance. The AE resistance was then evaluated at four different pressure levels (140, 270, 400 and 530 kPa at 1 MHz) as displayed in figure 5(b). The best fit line of the AE resistances at four pressures gave rise to $\Delta R/\Delta P$, which is the slope denoted in figure 5(c). This, combined with ρ_0 and part I in (3), was used to determine K. In this case, K equals 0.037%/MPa for 0.9% NaCl.

The same method was carried out at concentrations of 0.3%, 0.6%, 0.9%, 1.2% and 1.5% for both NaCl and $CuSO_4$ solutions. Figure 6(a) depicts different effects of K with concentration for monovalent (NaCl) and divalent ($CuSO_4$) salts. The difference is indicated by the slope and R^2 values for the two salts. For the monovalent NaCl, the small slope (0.003/MPa) and regression coefficient ($R^2 = 0.12$) suggested that K had no dependence on concentration. On the other hand, K for the divalent salt $CuSO_4$, with R^2 of 0.97 and a slope of 0.05/MPa, was highly dependent on concentration. Figure 6(b) portrays the signal amplitude measured with UCSDI for the two salts. It is clear, therefore, that for the monovalent salt NaCl, the AE signal does not depend on concentration, but for the divalent salt $CuSO_4$, it is very sensitive to concentration.

4.2. K in cardiac tissue

Typical UCSDI images (hot colors) and co-registered PE (gray) images across and along a strip of rabbit heart muscle are displayed in figure 7 (first and second column). In the third column, radiofrequency traces associated with the center of the UCSDI and PE images are illustrated. Stronger signals appeared at the tissue–air interface than the tissue–water interface because the former included a stronger reflection of the acoustic wave due to the acoustic impedance mismatch. The depth of the AE signal was converted from the one-way propagation of the ultrasound beam, while the depth of the PE signal was based on the two-way propagation. The frequency of the AE signal appears different from PE only because they are presented on a spatial scale. Figure 8 demonstrates the frequency response (Fourier transform) of the AE

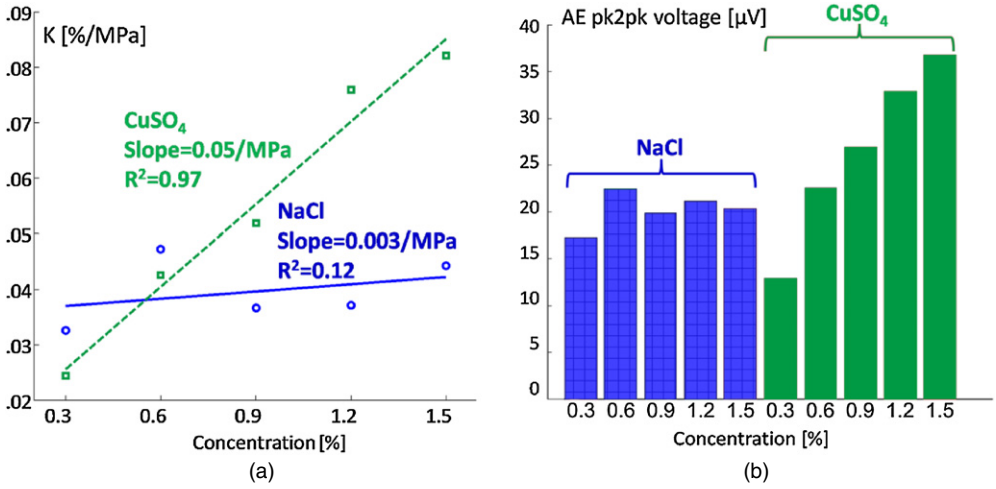

Figure 6. Comparison between NaCl and $CuSO_4$. (a) The same process demonstrated in figure 5 (a), (b) and (c) was repeated for different concentrations of NaCl and $CuSO_4$. The $\Delta R/\Delta P$ values are inserted into (3) to obtain the K values for different situations. The linear regression coefficients R^2 for K at different concentrations of NaCl and $CuSO_4$ were 0.12 and 0.97, respectively. (b) Amplitude of AE signals recorded at different concentrations for NaCl and $CuSO_4$.

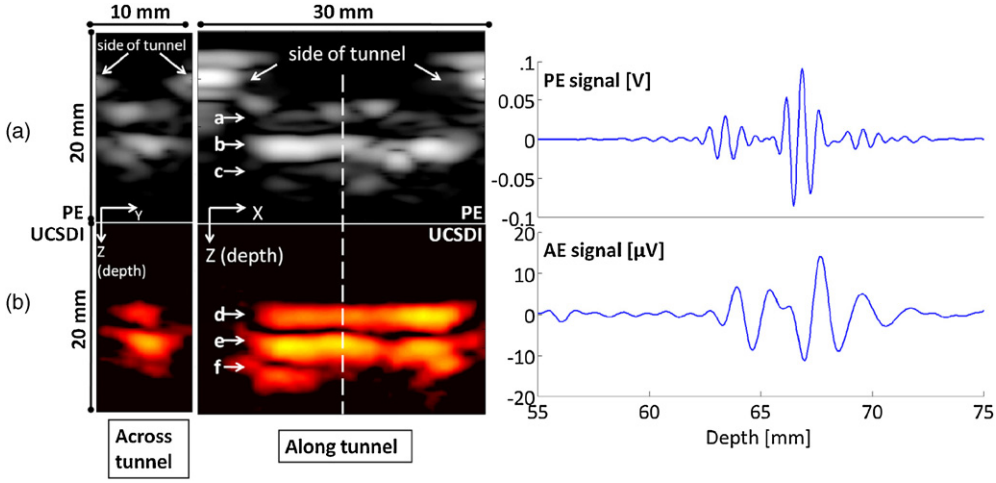

Figure 7. Signals and images of a strip of rabbit heart muscle with X along the direction of the tunnel, Y across the tunnel and Z as the depth direction. (a) First and second columns: B-mode PE images across and along the tunnel under a peak focal pressure of 530 kPa. Arrow 'a' points to the tissue–water interface, 'b' the tissue body and 'c' the tissue–air interface. The side of the tunnel is visible in the PE images. The third column is the corresponding PE signal marked by the white dashed line. (b) First and second columns: hot/cold color UCSDI images across and along the heart muscle under pressure of 400 kPa. Arrow 'd' points to the tissue–water interface corresponding to 'a' in the PE image. Arrow 'e' denotes the tissue–air interface, which is at the same position as 'c' in the PE image. Arrow 'f' points to the artifact due to the reflection of the acoustic wave. The third column represents the corresponding AE signal marked by the white dashed line.

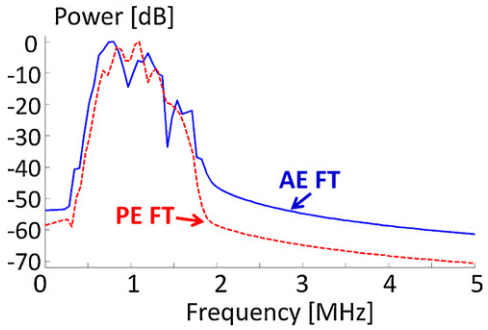

Figure 8. The power spectrum of the AE (blue solid line) and PE (red dashed line) signal traces demonstrated in the third column of figure 7. Each curve is scaled to its maximum magnitude in dB.

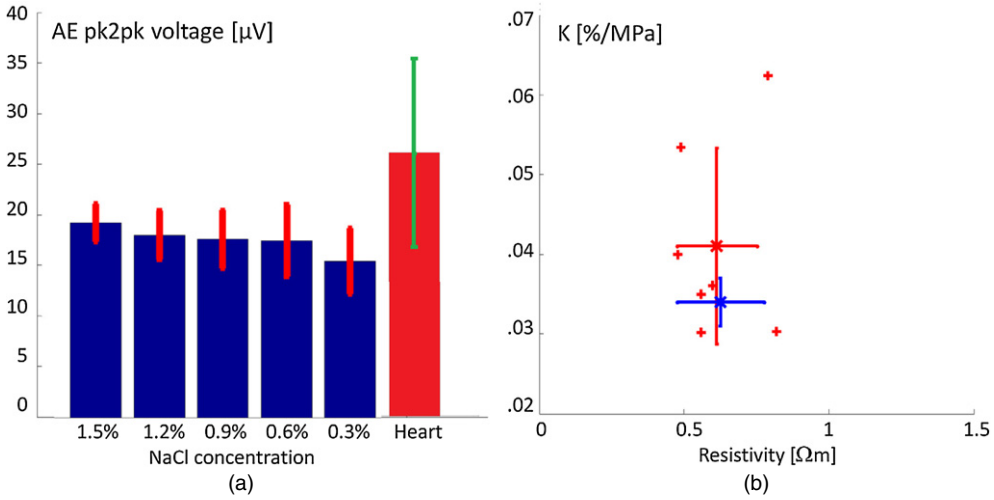

Figure 9. (a) Bar graph of the average AE peak-to-peak amplitude of seven hearts at 24 °C compared to the AE peak-to-peak amplitude measured in different concentrations of saline. Standard deviation of the values is depicted on top of the bars. (b) Distribution of K at 24 °C with respect to resistivity for all seven hearts (red crosses). Mean and standard deviation for the hearts (red X) compared to 0.9% saline (blue X) are also depicted.

and PE signal traces in the third column of figure 7. The frequencies of AE and PE signals evidently fall in the same spectral range, both centering at 1 MHz, the center frequency of the ultrasound transducer.

We measured K in seven different rabbit hearts. Using the same method as demonstrated previously for 0.9% saline, we calculated that the averaged AE signal in the heart was $26 \pm 9\ \mu$V. This value was compared to the AE signal amplitude in saline, which was measured in five samples per concentration, as illustrated in figure 9(a). The distribution of K with respect to resistivity for the seven rabbit hearts is plotted in figure 9(b). The red X denotes the mean value of K ($K = 0.041 \pm 0.012\%/\text{MPa}$) at the mean resistivity for the rabbit hearts. The K for 0.9% saline is also marked on figure 9(b) for comparison. The blue X denoted the mean value of K ($K = 0.034 \pm 0.003\%/\text{MPa}$) at the mean resistivity for 0.9% saline.

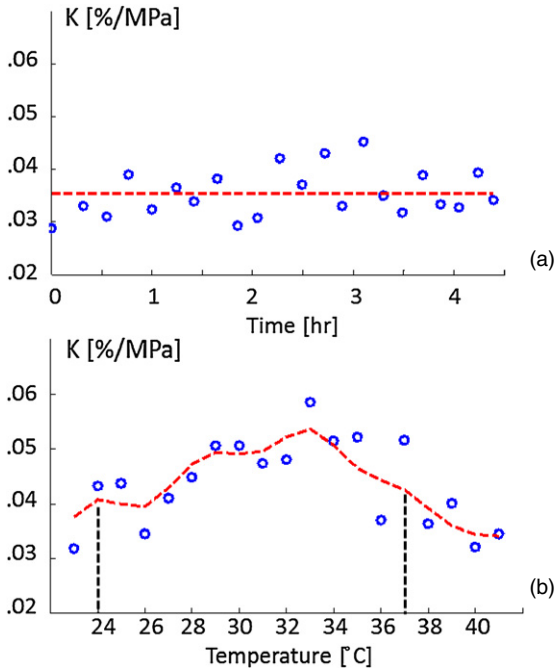

Figure 10. (a) K measured at 24 °C during a 4.5 h time window following tissue extraction. There was no particular trend relative to the mean ($0.035 \pm 0.0045\%/\text{MPa}$, denoted by red dashed line). (b) K measured at different temperatures. Red dashed line represents a Gaussian moving average (four points) through the data. Although there was a modest increase and decrease of K within this temperature range, K at room temperature ($0.041\%/\text{MPa}$) and body temperature ($0.042\%/\text{MPa}$) were very similar.

Figure 10(a) indicates that the measurement of K was relatively stationary during the first 4+ h of recording ($0.035 \pm 0.0045\%/\text{MPa}$). This suggests that the biological state of the excised tissue did not change appreciably during this time period, at least in terms of the passive acoustic and electric properties. Figure 10(b) depicts the trend in the value of K as the temperature of the tissue varied between room and body temperature. Although there is a steady increase followed by a decrease between these temperatures, the value of K at 24 °C ($0.041\%/\text{MPa}$) was very similar to the value at 37 °C ($0.042\%/\text{MPa}$).

5. Discussion

This study described a system to measure K in ionic solutions and cardiac tissue. In electrolytes, we observed very different behavior for K in NaCl and $CuSO_4$. The degree of dissociation of ions in solution affects the modulation of resistivity generated by the acoustic wave, resulting in different behavior with concentration. The concentration dependence of K for the salt $CuSO_4$ can be explained by its divalent bonding and incomplete disassociation in solution. This was not observed for NaCl, a monovalent salt, because its disassociation is essentially independent of concentration. This behavior was predicted by Koerber, although never verified experimentally (Koerber 1909).

We also provide the first estimates of K in fresh cadaver heart tissue. Our estimate of K in 0.9% saline ($0.034 \pm 0.003\%/\text{MPa}$) is within the range of previous published values

(0.01–0.1%/MPa, Jossinet *et al* 1998, 1999, Lavandier *et al* 2000a, 2000b). The K value in the heart ($0.041 \pm 0.012\%$/MPa) also falls in the same range. Physiological saline contains 0.9% NaCl, which is approximately the salt concentration in extracellular fluid and blood. This likely explains why the K values in 0.9% saline and cardiac tissue are similar. In figure 9(b), the blue and red vertical bars represent the standard deviation for the K measurement in 0.9% saline and rabbit hearts, respectively. While the blue error bar measured in saline primarily indicates system error, the larger red error bar suggests a greater variation for K in cardiac tissue. Differences between individual hearts and tissue preparation (e.g. fiber orientation in the tissue sample when placed in the tunnel) may have contributed to the total variability.

There are other factors that potentially affected our measurement of K. The tissue was maintained at room temperature (24 °C) rather than body temperature. However, results from an additional heart tested across a range of temperatures indicated that the values of K at 24 and 37 °C were similar, although we observed a trend between these temperatures. The amplitude of the AE signal as a function of temperature has been examined at cooler temperature in sea water, and there was no predictable trend observed (Fox *et al* 1946).

In conclusion, this study has reported the first measurement of the acoustoelectric interaction constant K in cardiac tissue as $0.041 \pm 0.012\%$/MPa. It is in accordance with our expectation of it being close to the value of K in physiological saline. This parameter is important because it provides a baseline of the sensitivity of UCSDI for mapping bioelectricity, such as reentry currents during treatment of arrhythmias, and can be included in heart modeling studies.

Acknowledgments

This study was supported by National Institute of Health (R01EB9353). We would like to thank Professor Terry Matsunaga at University of Arizona for his assistance in the animal preparation.

References

Duru F 2002 CARTO three-dimensional non-fluoroscopic electroanatomic mapping for catheter ablation of arrhythmias: a useful tool or an expensive toy for the electrophysiologist? *Anadolu Kardiyol Derg.* **2** 330–7

Fox F E, Herzfeld K F and Rock G D 1946 The effect of ultrasonic waves on the conductivity of salt solutions *Phys. Rev.* **70** 329–39

Gendron M, Guardo R and Bertrand M 2009 Experimental setup for developing acousto-electric interaction imaging *Conf. Proc. IEEE Engineering Medicine Biology Society* pp 2279–83

Jossinet J, Lavandier B and Cathignol D 1998 The phenomenology of acousto-electric interaction signal in aqueous solutions of electrolytes *Ultrasonics* **36** 607–13

Jossinet J, Lavandier B and Cathignol D 1999 Impedance modulation by pulsed ultrasound *Ann. NY Acad. Sci.* **873** 396–407

Koerber F 1909 Über den einfluss des druckes auf das elektrolytische leitvermögen von Lösungen *PhD Dissertation* Department Physical Chemistry, Göttingen, Germany

Lavandier B, Jossinet J and Cathignol D 2000a Quantitative assessment of ultrasound-induced resistance change in saline solution *Ultrasonics* **38** 150–5

Lavandier B, Jossinet J and Cathignol D 2000b Experimental measurement of the acousto-electric interaction signal in saline solution *Ultrasonics* **38** 929–36

Li Q, Olafsson R, Ingram P, Wang Z and Witte R 2010 Measuring the acoustoelectric interaction constant in cardiac tissue using ultrasound current source density imaging *IEEE Int. Ultrasonics Symp. (San Diego)* pp 245–8

Markides V and Davies D W 2005 New mapping technologies: an overview with a clinical perspective *J. Intervent. Cardiac Electrophysiol.* **13** 43–51

Olafsson R, Witte R, Huang S-W and O'Donnell M 2008 Ultrasound current source density imaging *IEEE Trans. Biomed. Eng.* **55** 1840–8

Olafsson R, Witte R, Jia C, Huang S-W, Kang K and O'Donnell M 2009 Cardiac activation mapping using ultrasound current source density imaging (UCSDI) *Ultrason. Ferroelectr. Freq. Control* **56** 565–74

Packer D L 2005 Three-dimensional mapping in interventional electrophysiology: techniques and technology *J. Cardiovasc. Electrophysiol.* **16** 1110–6

Wang Z, Olafsson R, Ingram P, Li Q and Witte R 2010 Multichannel ultrasound current source density imaging of a 3D dipole field *IEEE Int. Ultrasonics Symp. (San Diego)* pp 253–6

Witte R, Olafsson R, Huang S-W and O'Donnell M 2007 Imaging current flow in lobster nerve cord using the acoustoelectric effect *Appl. Phys. Lett.* **90** 163902

Zhang H and Wang L 2004 Acousto-electric tomography *Proc. SPIE* **5320** 145–9